SPACE TELESCOPE SCIENCE INSTITUTE
Operated for NASA by AURA

Instrument Science Report WFC3 2014–18

Pixel-to-Pixel Flat Field Changes in WFC3/UVIS

H.Gunning, S. Baggett, J. MacKenty
Space Telescope Science Institute
September 9, 2014

ABSTRACT

During the time between anneals, an evolving population of pixels with lowered sensitivity develops. The population is wavelength dependent: the bluer wavelengths appear to have more pixels with lower sensitivity than the redder wavelengths. Preliminary analysis of the population in the UV indicates the low sensitivity pixels typically exist in groups with sizes of a few pixels; at redder wavelengths, these pixels are normally isolated single pixels. The population appears to be a unique set with each anneal cycle and shows no evidence of being a pure population of pixels that 'telegraph' between having low and normal sensitivity. Like the WFC3/UVIS hot-pixel population, the annealing process appears to reset a fraction of the low-sensitivity population (in this case, 90%). Most pixels deviating by $\sim$ –1% recover within a single anneal, however deviations of more than –2% can require more than one anneal to recover to within 1% of their median value.The total population of pixels deviating by more than 2-3% currently ranges from 0.1% in F814W and F438W and from $\sim$ 3% up to $\sim$ 10% in F225W, depending upon time since the anneal procedure. Spontaneous recovery of sensitivity in isolated low-sensitivity pixels has been observed. The extent of full recovery after a lowered-sensitivity event is not fully understood, more data will be required to monitor the population evolution and behavior over longer time frames and larger a wavelength range.

1 Introduction

The WFC3 UVIS channel consists of two 2051x4096 silicon-based detectors assembled in a 2x1 mosaic. Once a month the UVIS detector is warmed to $\sim$ 20C (an 'anneal' procedure), which currently successfully fixes 70-80% of the hot pixel population that develops during the time between anneals.

The complete history of UVIS anneals can be found at http://www.stsci.edu/hst/wfc3/ins_performance/monitoring/UVIS/anneal.html. In addition to the hot-pixel population, there exists another population of pixels with transient pixel-to-pixel sensitivity that cannot be explained through noise statistics.

A similar population exists in ACS/WFC and is quantified in the ACS ISR 2007-01 by Gilliland et al. In this report we will discuss the lowered sensitivity of this anomalous population in WFC3, how we identify pixels with lowered sensitivity, their correlation with the monthly anneals, wavelength dependence, sensitivity recovery, and mitigation options.

2 Method

The data analyzed in this report are from calibration proposal 13169, a cycle 20 program designed specifically to identify and track these variant pixels. The 24-visit program utilizes both UV (F225W, F336W) and visible (F438W, F814W) filters to cover most of the wavelength range of the detector. We obtained 19 visits of F438W and F814W, and 6 visits of F225W and F336W. Each visit of the visible filters is begun with a UVIS1-M512-SUB subarray exposure through the F645N filter to warm the lamp, ensuring the lamp intensity across visits is uniform. After the lamp-warming exposure, 8 exposures are obtained, 4 in each of F814W and F438W. For each visit of the UV filters, 3 exposures of F336W, and 4 exposures of F225W are obtained. We omit to warm the Deuterium lamp at the beginning of the UV visits to reduce the cycling of the limited-lifetime lamp. Examples of internal flats are shown in Figure 1 and a detailed table of exposures is given at the end of this document in Table A. All data analyzed in this report were processed through the standard archive pipeline with the most up-to-date biases and darks for their respective observation dates.

Our analysis is similar to that which was used to identify and track a similar population on ACS WFC; we retrieve our data as _flt.fits files, eliminate cosmic rays over 3-4 exposures per visit and create an average per-visit image. With all _flt.fits files from the calibration proposal for a given filter, we generated a median FLT to be used as the 'ideal' detector - a baseline from which we can calculate pixel sensitivity deviations. To ensure the deviant pixels we identify are indeed lowered efficiency pixels, we set the limit for low-sensitivity pixels higher than known contributors of noise. We also ignore the top and bottom 10 rows on each chip. The median flat data for F814W, F438W, F336W, and F225W used in our analysis are shown in Figure 1 and labeled as 1(a), 1(b), 1(c),and 1(d), respectively. Figure 2 shows a 400x400 pixel region on chip 2 in all four filters. Dust can clearly be seen in all filters, but the UV filters, F336W and F225W, have significantly more. The next zoomed-in region in Figure 3 shows a 100x100-pixel region on chip 2. F814W and F438W are relatively flat, with no strong features, while F336W and F225W both show a strong dust moat.

3 General Characteristics

The lowered-efficiency pixels are identified by the deviation from the median 'ideal' flat. The main source of variation we take into consideration with the internal flat fields is the lamp intensity. The WFC3 default tungsten lamp intensity varies by approximately 0.4%(Bourque 2013). The tungsten lamp is used

specifically for the F814W and F438W (visible) flats while the deuterium lamp is used for the F336W and F225W (UV) flats.The UV flats contain more features than the visual flats, the 'droplet' like features are best seen in Figure 2. WFC3 ISR 2008-17 (Sabbi) provides a complete atlas of the internal flat fields. Note that the collimated beam (f/300) of the internal calibration lamp causes the droplets to appear significant in the internal flats. In science data (taken at f/31), the droplets become more diffuse and their effect on

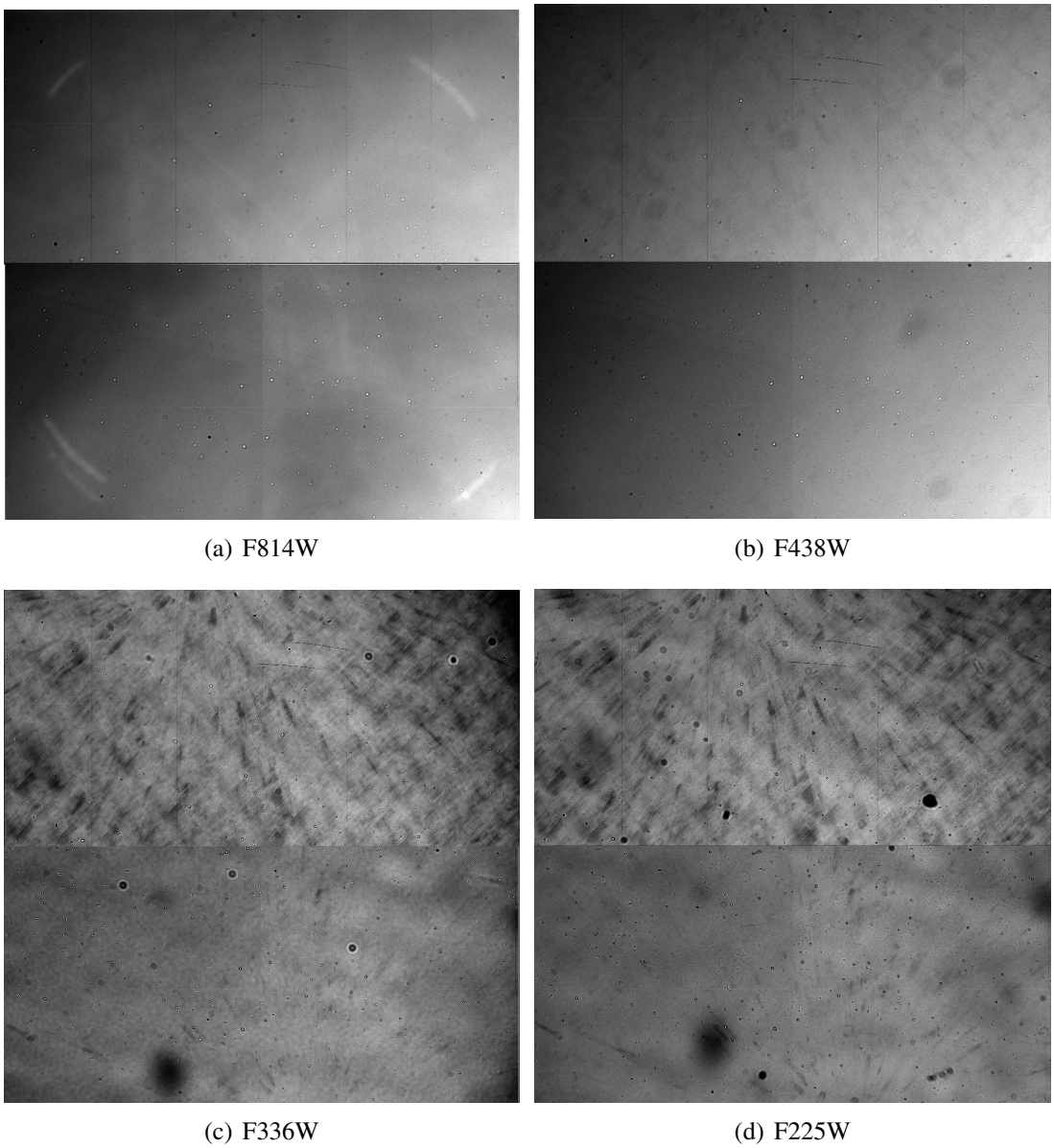

(a) F814W (b) F438W

(c) F336W (d) F225W

Figure 1: Median Flats for F814W (upper left), F438W (upper right), F225W (lower right), and F336W (lower left). Chip 1 is the top half and chip 2 is the bottom half of all flat frames shown. Each chip (in each filter) is shown with a $\pm$20% stretch. Note the prominent cross-hatch pattern in the UV filters in chip 1. The arc features in the corners of the F814W flat are artifacts of the calibration subsystem used to obtain the flats.

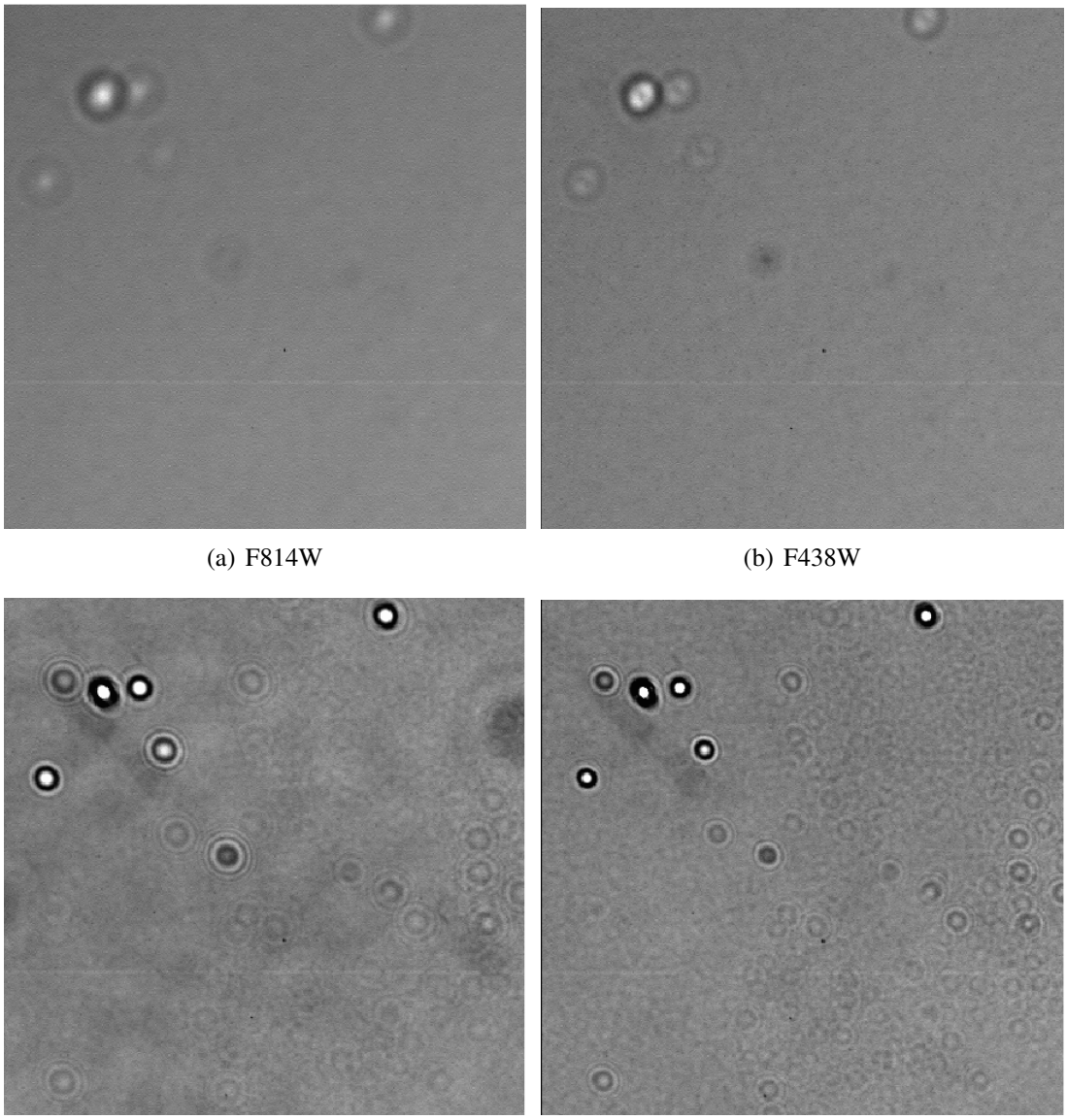

(a) F814W (b) F438W

(c) F336W (d) F225W

Figure 2: 400x400 section of Median Flats for F814W (upper left), F438W (upper right), F225W (lower right), and F336W (lower left). Shown with $\pm$ 20% stretch. In the highly collimated beam of the internal flat field deuterium lamp, the 'droplets' appear in the UV flats as high contrast features some 10's of pixels in diameter. The effect of the droplets on science data is minimal but they can generate false positives in the identification of lower-sensitivity pixels.

has been shown to be minimal. That is, in large-aperture photometry (>10 pixel radius), the droplets have effectively no impact while in small aperture photometry ($\sim$3 pixel radius), the droplets increase the photometric scatter from 0.5% to 1% (Brown et al., 2008).

science data. Other sources of variation that we have not been able to completely identify add noise to the pixel-to-pixel variations over time. Thus, for nearly all filters, the cut-off for identifying a pixel as having

a lower sensitivity has been set at -1%, the approximate value for poisson noise for our data. Due to the higher noise in F225W, the cut-off in that filter has been set at –3%. Along with the droplets, the UV filters have more dust-like features (see Figures 2 and 3), which contribute to noisiness in the median. These differences cause greater deviations and hence require a relaxed lower limit to ensure that we are correctly identifying pixels with low sensitivity and not just small deviations in the locations of dust motes. The statistics of the populations for each visit are given in Tables 1, 2, 3, 4 for filters, F814W, F438W, F336W, and F225W, respectively.

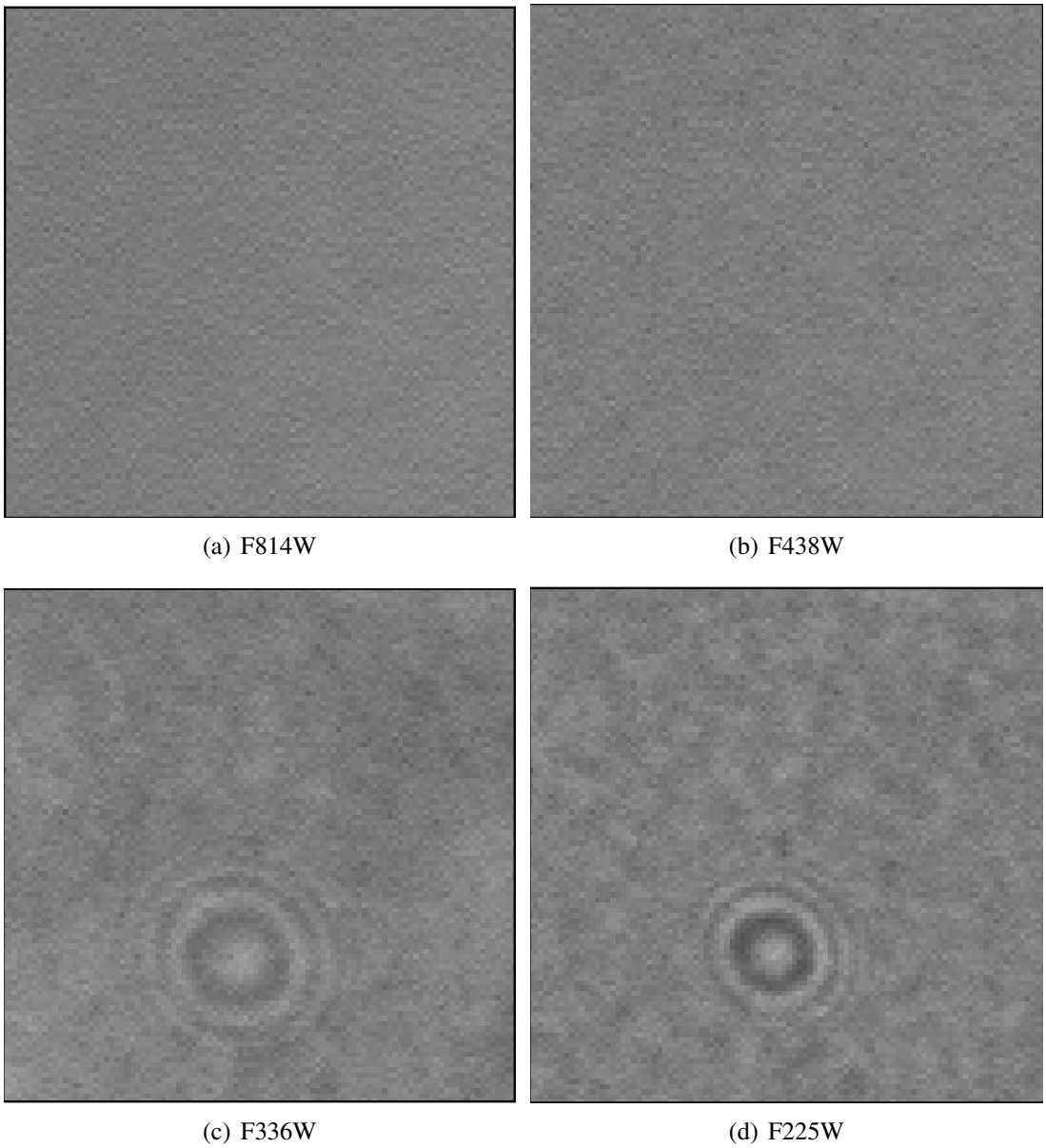

(a) F814W (b) F438W

(c) F336W (d) F225W

Figure 3: 100x100 section of Median Flats for F814W (upper left), F438W (upper right), F225W (lower right), and F336W (lower left). Shown with $\pm$ 20% stretch. The large bulls-eye in the UV filter images is a droplet feature.

4 Effect of Anneals on Low Sensitivity Pixels

In Figures 4 and 5 the total normalized low-sensitivity pixel counts for pixels in bins of –1%, –2%, and –4% are plotted as a function of time to show how the pixel population evolves before and after anneals, which are indicated by the vertical black lines. For both F438W and F814W, the low-sensitivity population grows during the time between anneals and approximately 90% of these are reset by the anneal. The –2% (green) and –4% (purple) populations reset after each anneal and exhibit nearly the same population patterns. The population within the –1% bin (blue line in figures 4 and 5) do not necessarily show a reset after each anneal. Specifically for F814W, the second anneal does not reset the population, instead the lowered-sensitivity population increases after the anneal for the $\leq$ –1% bin. For Figure 4, F438W, the lack of reset is seen in the second-to-last anneal where the low-sensitivity population continues to grow after the anneal. The lack of consistent reset trend for the $\leq$ –1% in both filters suggests the pixels flagged in this bin are not homogeneous and contain pixels deviating for reasons other than pure low sensitivity. The stronger pattern in the pixels deviating by $\leq$ –2% suggests we get a better homogeneous sample of low sensitivity pixels. While we didn't have the cadence to determine the rate of growth during the time between anneals, we can see that the population deviating around the $\sim$ –1% grows significantly more in

Date	Visit	< –1%	< –2%	< –4%
2-Dec-12	v01	116944	7875	17
6-Dec-12	anneal			
9-Dec-12	v03	17864	489	1
29-Dec-12	v05	51198	4542	10
1-Jan-13	anneal			
7-Jan-13	v07	78712	2571	6
17-Jan-13	v08	205095	7421	17
26-Jan-13	v09	73088	7472	14
29-Jan-13	v10	181743	10159	27
31-Jan-13	anneal			
3-Feb-13	v11	69092	1153	4
13-Feb-13	v12	83942	4750	11
22-Feb-13	v14	98658	9076	26
25-Feb-13	v13	240718	13467	54
28-Feb-13	anneal			
6-Mar-13	v15	15368	1297	6
14-Mar-13	v16	50666	4550	19
23-Mar-13	v18	177611	12073	95
25-Mar-13	v17	272315	13960	99
26-Mar-13	anneal			
31-Mar-13	v19	115623	3536	61
20-Apr-13	v21	118206	14561	147
26-Apr-13	anneal			
29-Apr-13	v23	128383	2888	46

Table 1: Deviant pixel population counts for F814W internal flats

Date	Visit	< –1%	< –2%	< –4%
2-Dec-12	v01	117910	38962	5831
6-Dec-12	anneal			
9-Dec-12	v03	12056	3445	574
29-Dec-12	v05	149542	43736	7020
1-Jan-13	anneal			
7-Jan-13	v07	26239	9271	1812
17-Jan-13	v08	153034	35944	6426
26-Jan-13	v09	164746	50766	8972
29-Jan-13	v10	118552	42403	7762
31-Jan-13	anneal			
3-Feb-13	v11	26504	6127	1175
13-Feb-13	v12	134703	31084	5470
22-Feb-13	v14	171822	53271	9549
25-Feb-13	v13	193352	59659	10528
28-Feb-13	anneal			
6-Mar-13	v15	31826	8670	1561
14-Mar-13	v16	62398	20508	2795
23-Mar-13	v18	141409	46099	8759
25-Mar-13	v17	194265	54134	10150
26-Mar-13	anneal			
31-Mar-13	v19	228908	20294	3868
20-Apr-13	v21	266976	76928	16757
26-Apr-13	anneal			
29-Apr-13	v23	97327	18760	2418

Table 2: Deviant pixel population counts for F438W internal flats

each filter than the pixels deviating by < –2%. These limits are purely arbitrary and were simply chosen as proxy values to eliminate as many false positives as possible when selecting the low sensitivity pixel population.

Much like the hot pixel-population in the UVIS detectors, the low-sensitivity population of pixels that develops over the time between anneals seems to largely reset after the annealing process, which is done monthly. This trend is very evident in the population deviating by $\leq$ –2%, our most homogenous sample. The closer a data set is taken after an anneal, the less contamination from these low sensitivity pixels exists. Although, even the largest population bins affect only a relatively small fraction of pixels, « 0.5% of the chip in F814W and F438W, and 3% up to $\sim$10% in F225W (in the $\leq$ –3% bin). For comparison, about 3.5% of the pixels are considered "hot". The wavelength dependence of the low-sensitivity pixels will be discussed in a later section. Total population trends in each filter suggest that for the small amount of the detector afflicted with low-sensitivity pixels, most recover after an anneal. Longer monitoring of these trends will have to be done to determine if, like ACS, the permanent population is slowly growing with time (Gilliland 2007).

Date	Visit	< –1%	< –2%	< –4%
4-Dec-12	v02	324155	46991	7254
9-Dec-12	v04	21318	3262	642
29-Dec-12	v06	339886	51487	8434
31-Mar-13	v20	73307	9130	1614
20-Apr-13	v22	638391	76001	14600
29-Apr-13	v24	221091	25372	2183

Table 3: Deviant pixel population counts for F336W internal flats

Date	Visit	< –3%	< –4%	< –5%
4-Dec-12	v02	366368	18920	4910
9-Dec-12	v04	14663	2022	460
29-Dec-12	v06	243587	27553	8106
31-Mar-13	v20	170985	11174	3206
20-Apr-13	v22	1003428	52638	13437
29-Apr-13	v24	463276	12762	2196

Table 4: Deviant pixel population counts for F225W internal flats

5 Repeat Offenders

The initial goal of the calibration program was to determine whether WFC3/UVIS has a population of low sensitivity pixels and if so, to characterize their behavior. To address this, we must determine whether the population is unique each visit or whether pixels low in one visit are consistently low in subsequent visits, i.e. the pixels would be the same set that flip between low and normal sensitivity. We inspected our populations at each visit and made a 3-dimensional data cube, (x,y,z) = (4096,2051,18), for each UVIS chip and populated each extension (0-17) with the location of each identified anomalous pixel with a value of 1.0. In the end we were able to sum over our data cube and obtain a final (4096,2051), per chip, array that identified how many times at each pixel location was a pixel identified with low sensitivity with respect to the median 'ideal' flat. Tables 5 and 6 summarize our results. The left column of each table is the maximum number of times each pixel is found to occupy the respective percentage bin. For example, in Table 5, the number of pixels that only occur once (No. repeat = 1) with deviations $\leq$ –1% is 1387320. The number of low sensitivity pixels that deviate $\leq$ –4% and repeat 3 times within our time frame is 10.

For the F814W pixels, in the $\leq$ –1% bin, 83% of low QE pixels only occur once then recover, in the $\leq$ –2% bin 62% occur once and recover, and in the $\leq$ –4% bin 67% occur once and recover. *This indicates that the majority of the population in F814W occur once and recover normal sensitivity.* If we include hits

1 and 2, the percentage for $\leq$ –1%, $\leq$ –2%, and $\leq$ –4% becomes 94%, 85%, and 82%, respectively. For the F438W pixels, in the $\leq$ –1%, $\leq$ –2%, and $\leq$ –4% bins, only 59%, 55%, and 58%, respectively, occur once and recover. If we include hits 1 and 2, the percentage jumps to ~80%. *Although the majority of low sensitivity pixels in both filters do recover their sensitivity back to the noise range of the median flat, not all achieve this with just one anneal.*

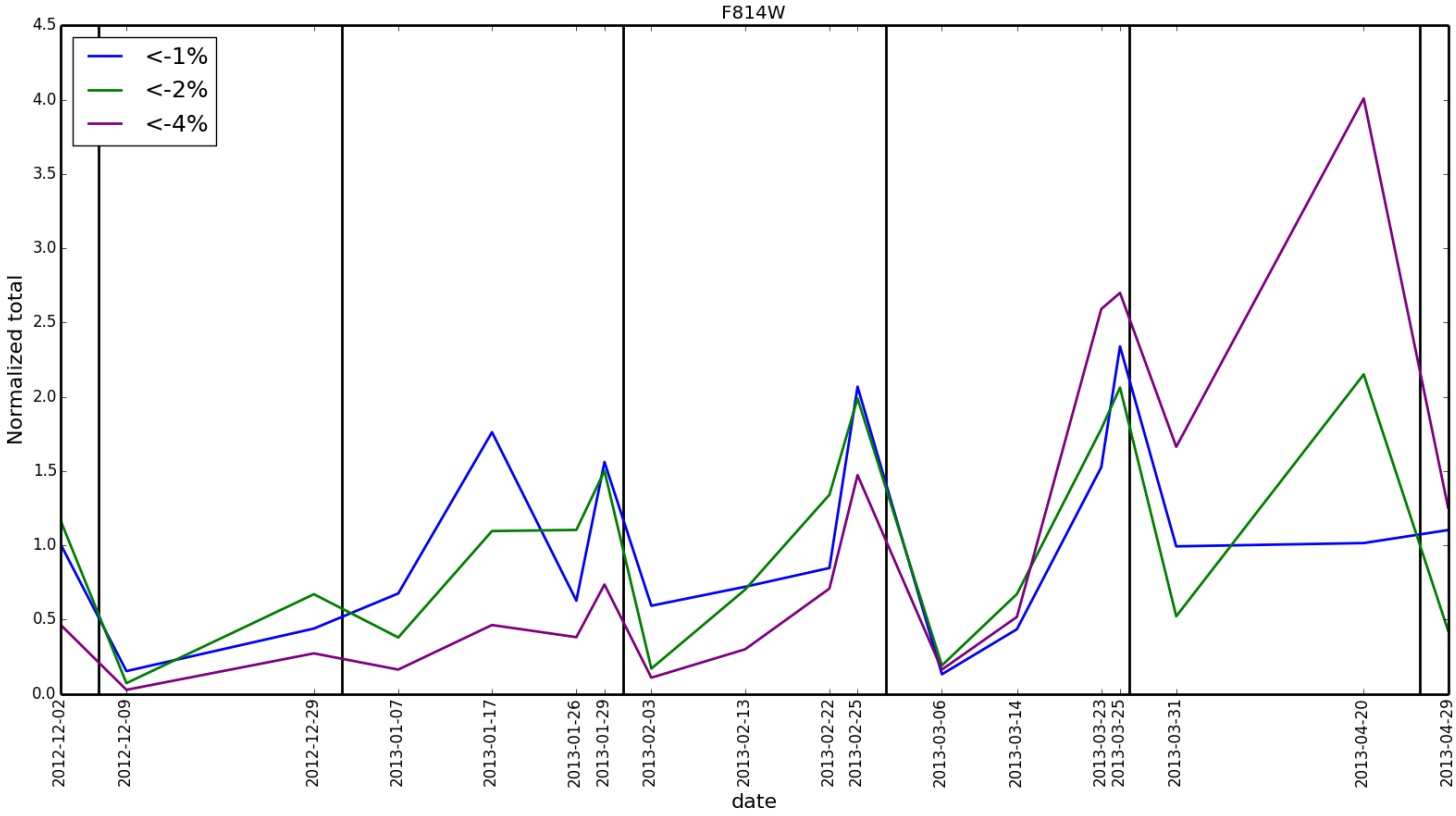

Figure 4: Normalized low sensitivity pixel population in the F814W filter as a function of time. Anneals are indicated by black vertical lines, deviations $\leq$ –1%, $\leq$ –2%, and $\leq$ –4% populations are shown by the blue, green, and purple lines, respectively.

6 Wavelength Dependence

To explore how the population behaves from filter to filter, we matched all flagged low QE pixels between the F814W and F438W filters per each observed visit. Table 7 summarizes the quantity matched and the percentage of the total flagged low QE pixels in F814W that were matched with the population from F438W. For all pixels varying by $\leq$ –1% the average percent match (of the F814W population) was 42%, i.e., 42% of the low QE pixels identified in F814W were also low in F438W. For the $\leq$ –2% population, nearly every low sensitivity pixel in F814W was found to have low sensitivity in F438W. However, the total number of low QE pixels is higher in F438W than in F814W beyond the $\leq$ -2% level and has more repeat offenders across all percentage bins, indicating that that the population increases with bluer filters,

as grouping behavior becomes stronger, and the pixels on average take longer to recover in F438W than in F814W. A more in-depth discussion of grouping in the UV will be included in the next ISR.

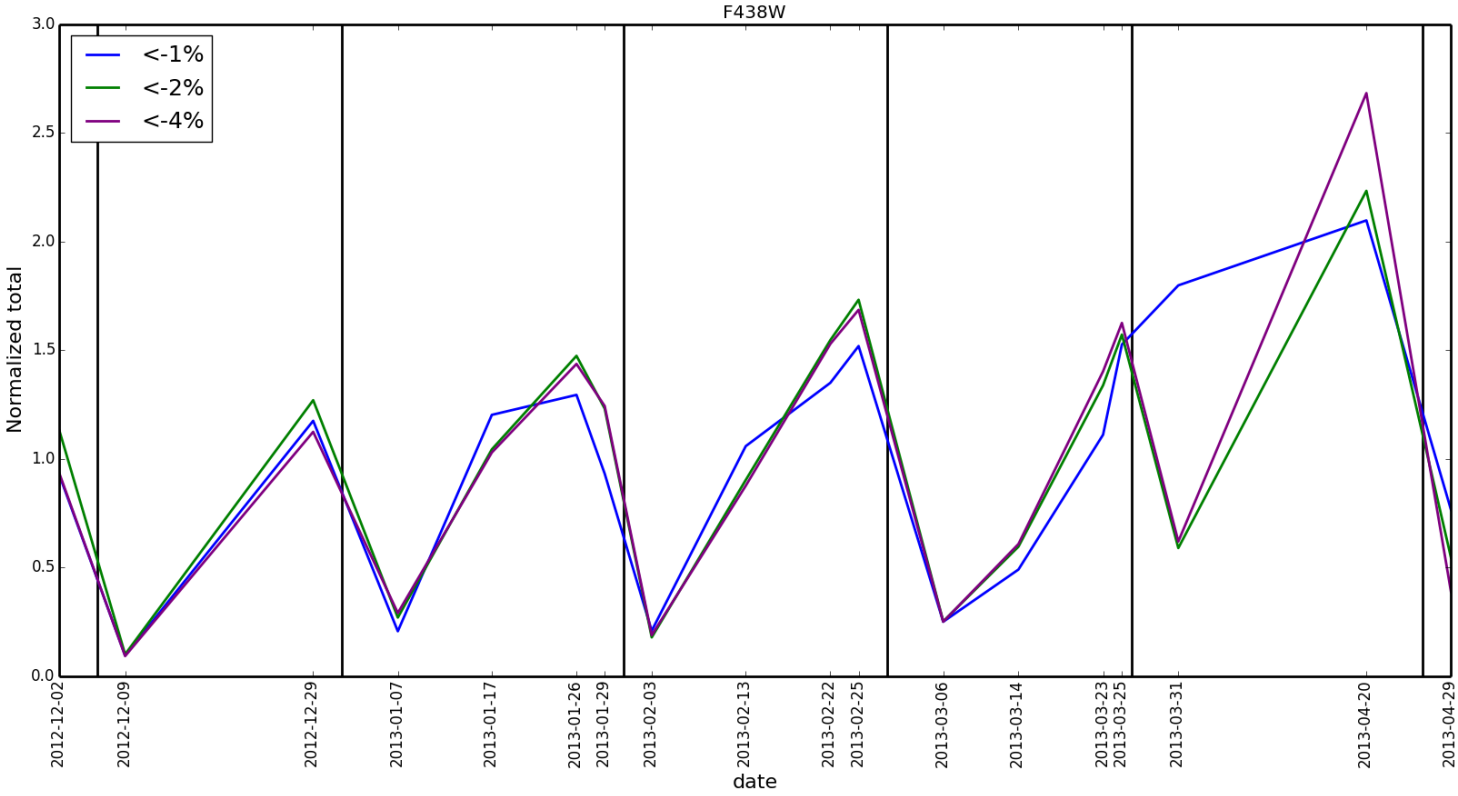

Figure 5: Normalized low sensitivity pixel population in the F438W filter as a function of time. Anneals are indicated by black vertical lines, deviations $\leq$ -1%, $\leq$ -2%, and $\leq$ -4% populations are shown by the blue, green, and purple lines, respectively

Figures 8 and 9 show a 3x3 pixel region on amp A in chip 1 in both F814W and F438W filters, respectively, over the timeline of our observations from cycle 20. The dark grey bar indicates the percent deviation $\pm$ 0.5% and the lighter grey bar indicates $\pm$ 1.0%, where the –1.0% is our cutoff for identifying a pixel with low sensitivity. The $\pm$ 1% deviation range henceforth will be called the "noise". The center frame in figure 8 shows a pixel that was identified as having low sensitivity with a percent deviation $\sim$ –1% in F814W. The same pixel (x=144,y=103) in F438W shown in figure 9 is not flagged over the same time frame as it is in F814W. This further supports that not all pixels in F814W that vary by $\sim$ –1% translate into other filters. Figures 10 through 13 show examples of pixel variations in F814W that are $\leq$ –2% that also have low sensitivity in F438W. These will be discussed in more detail in the next section. To better illustrate the wavelength dependence of pixels with low sensitivity in both F814W and F438W, we isolated a pixel population that exists in both filters with sensivity deficits $\leq$ –1%. In Figure 6, We show individual pixels with low sensitivity in both F814W and F438W. The percent deviation of the population in F438W is shown as a function of the percent deviation of the population in F814W. The red line represents no wavelength dependence, i.e.equal sensitivity levels in both filters. The population exhibits a greater slope than the red line, indicating that the deviations in F438W are approximately 2 times greater than in F814W.

Preliminary analysis of the F225W and F336W data indicates that the population that exists in the bluer filters also tends to cluster together in groups of a few pixels. UV programs that do not dither, or do not have a large enough dither pattern, may see effects from this population. The behavior of pixels with low sensitivity in the UV will require further investigation.

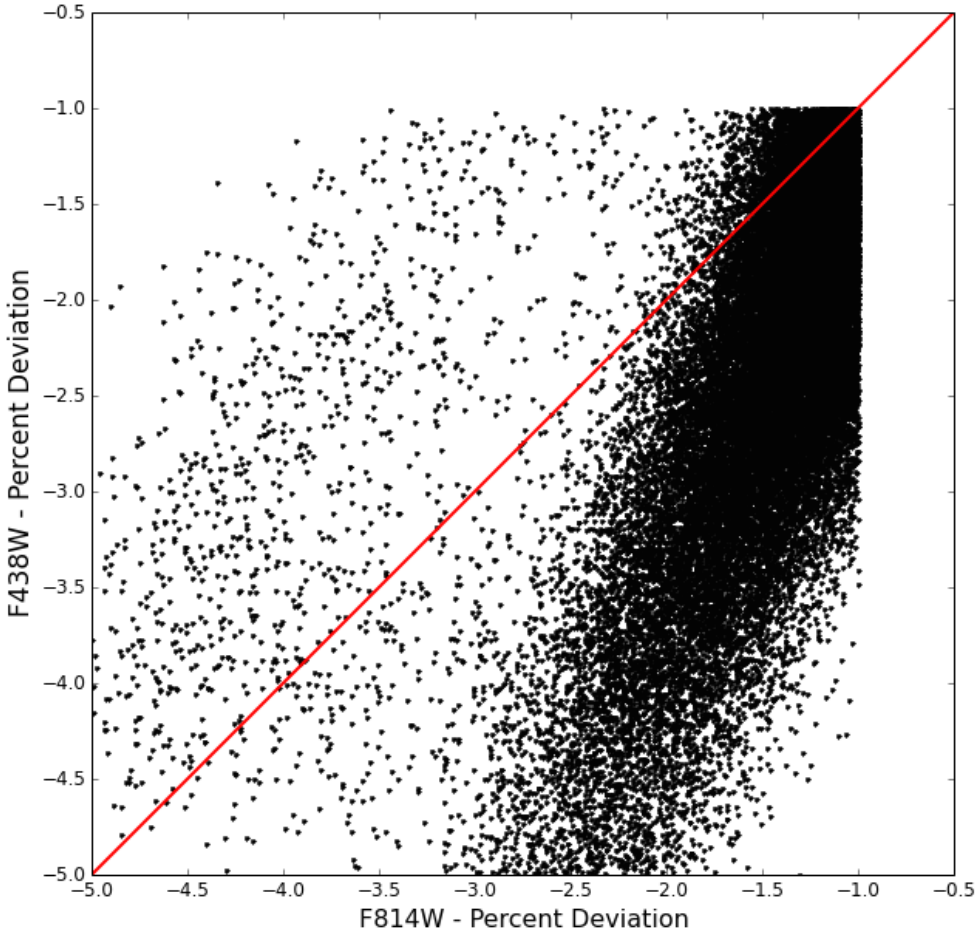

Figure 6: Individual pixels flagged with low sensitivity in both F814W and F438W. The percent deviation in F438W is shown as a function of the percent deviation in F814W. Low sensitivity pixels show more sensitivity loss in the blue (F438W) than in the red (F814W); the red line denotes equal sensitivity levels in both filters.

7 Sensitivity Recovery

Figures 8 through 13 show pixel variations for 3x3 regions surrounding a randomly selected low-sensitivity pixel, shown in red in each figure. The dark gray bar indicates ± 0.5% while the light grey bar indicates ± 1.0%, referred to later as the "noise". The same pixel region is plotted for both F814W and F438W filters. Figure 8 shows the region surrounding pixel 144,103 on chip 1 in the F814W filter. This pixel was identified to be anomalous around the –1% level on January 29, 2013 (indicated by the orange box), our

No. repeat	$\leq$ –1%	$\leq$ –2%	$\leq$ –4%
1	1387320	51523	446
2	187123	19006	84
3	67537	7957	10
4	25764	2084	4
5	3746	6	0
6	870	1	0
7	269	3	0
8	117	0	0
9	55	2	0
10	33	1	0
11	16	0	0
12	6	0	0
13	5	1	0
14	4	0	0
15	2	0	0
16	0	0	0
17	0	0	0
18	0	0	0

Table 5: Number of repeated deviant pixels for F814W. For example, the number of pixels that were deviant twice in the $\leq$ –1% bin was 187,123. The number of pixels that were flagged four times in the $\leq$ –2% bin was 2084.

No. repeat	$\leq$ –1%	$\leq$ –2%	$\leq$ –4%
1	763256	200290	40556
2	258481	86890	16792
3	144798	50294	8625
4	70519	20575	3042
5	22480	1177	18
6	9792	427	6
7	5631	221	4
8	3840	106	1
9	1976	69	2
10	1310	51	0
11	737	25	2
12	396	9	1
13	398	16	0
14	230	10	0
15	97	7	2
16	0	0	0
17	0	0	0
18	0	0	0

Table 6: Number of repeated deviant pixels for F438W. For example, the number of pixels that were flagged with low sensitivity once in the $\leq$ –4% bin was 40,556 and the number of pixels flagged four times in the $\leq$ –1% bin was 70,519.

observation just before the January 31st anneal. The low sensitivity of pixel 144,103 recovers within $\sim$ 1% of the median flat, but does not appear to recover to the same sensitivity level found prior to the deviation. Similarly, in Figure 9 the same region as Figure 8 is shown but in the F438W filter. The low sensitivity pixel identified in F814W is not flagged in F438W and neither are any surrounding pixels. This illustrates our earlier conclusion that not all the pixels that exhibit low sensitivity at the $\sim$ 1% level in F814W also show low sensitivity in F438W.

We also investigated pixel variations at $\leq$ –2% and $\leq$ –4% levels. Figure 10 and 11 show central pixel x=726, y=600 varying in both filters F814W and F438W, respectively. In the F814W filter, the pixel exhibits sensitivity about 0.5% higher than normal before becoming a low-sensitivity pixel and recovers partially after the 01/31/2013 anneal but doesn't recover completely until after the 04/26/2013 anneal (4 anneals after the pixel was identified as having low sensitivity). Furthermore, while we consider the pixel technically recovered since it rises to within 1% of the pixel's average level, note that the pixel never does reach the level of sensitivity it had before it went through the low QE phase. Unlike the previous case, the-low sensitivity pixel is also flagged in the F438W filter, varying by a greater percent deviation than it shows in the F814W filter. The pixel in both filters recovers back into the noise, but the F438W low sensitivity pixel recovers only partially after 2 anneals, and seems to not recover fully within our timeline. Most of the surrounding pixels in F814W do not deviate outside the $\pm$ 1% noise, but the pixel to the right of the central pixel does deviate to about -1.5%.

Visit	$\leq$ –1%	% F814W	$\leq$ –2%	% F814W	$\leq$ –4%	% F814W
v01	60136	51%	7773	99%	16	94%
v03	3612	20%	479	98%	1	100%
v05	36315	71%	4504	99%	8	80%
v07	14374	18%	2489	97%	6	100%
v08	51802	25%	7221	97%	17	100%
v09	52309	72%	7420	99%	12	86%
v10	64873	36%	9961	98%	25	93%
v11	7491	11%	1132	98%	3	75%
v12	34834	41%	4681	99%	11	100%
v14	64065	65%	9000	99%	25	96%
v13	93934	39%	13266	99%	52	96%
v15	10105	66%	1288	99%	4	67%
v16	29260	58%	4496	99%	18	95%
v18	75393	42%	11884	98%	93	98%
v17	86069	32%	13256	95%	89	90%
v19	27106	23%	3386	96%	51	84%
v21	80388	68%	14399	99%	121	82%
v23	31003	24%	2775	96%	38	83%

Table 7: Population numbers that match between filters F814W and F438W and the percent of all F814W low QE pixels that exist in the flagged F438W population. For example, in Visit v01, 60136 pixels were identified as having low sensitivity ($\leq$ –1% bin) in both F814W and F438W, accounting for 51% of the identified population in F814W. Similarly, 7773 pixels pixels were identified with low sensitivity ($\leq$ –2% bin) in F814W and F438W, accounting for 99% of the low sensitivity pixels in this bin for F814W.

The surrounding pixels in F438W seem to correlate more with the deviation than in F814W. In this bluer filter, there are three pixels that are also flagged as having low sensitivity during the same time between anneals as the central pixel, although none show quite the percent deviation as the central pixel. This is an example of the correlated grouping behavior of the low sensitivity pixels at bluer wavelengths.

Figures 12 and 13 show the 3x3 pixel region surrounding the central pixel x=600, y= 975 in both F814W and F438W filters, respectively. Figure 12 shows a deep decline $\sim$ –3% followed by further decline to $\sim$ –3.5% between the January 1st, 2013 and January 31st, 2013 anneals. The pixel recovers into the noise, but deviates slightly out of the noise before the 03/26/13 anneal then slips back into the noise before the anneal. The same pixel, in filter F438W, shows a slight positive deviation before declining on the same timescale as the F814W data. Again, this pixel declines between the January 2013 anneals, but is reset by the anneal on January 31st, 2013. Though the pixel resets in both filters back into the noise, over our timeframe the pixel does not seem to recover fully. Unlike the previous case, where the surrounding pixels were somewhat correlated in the F438W data, this particular low-sensitivity event doesn't exhibit clustering in either filter.

8 UVIS Comparison to the ACS WFC

As mentioned previously, the ACS Wide Field Camera (WFC) has a similar evolving low-sensitivity population. As reported in ACS ISR 2007-01, a population of low sensitivity develops but is largely reset by the anneal procedure. The ACS WFC experiences larger sensitivity deficits in the blue when compared to the red filters, with unique population sets each anneal cycle. They see low-sensitivity pixels recover approximately 90% of their sensitivity on a time scale of a few months. They note that less-frequent anneals would lead to larger sources of errors due to the continually-growing low-sensitivity population. See Figure 7 for a table of their values obtained from ACS ISR 2007-01 (Gilliland 2007), equivalent to Tables 1, 2, 3, and 4.

Table 1: Deviant pixel counts for the 24 F435W internal flats

Cal ID-Visit	Year	Time	≥4%	≥2%	≥1%	≤-1%	≤-2%	≤-4%
9562-02	2.31	24.5	246	1760	55527	97196	23360	2327
9562-10	2.56	7.0	214	1528	46887	36636	6197	680
9657-02	2.58	17.3	195	1425	39217	64363	15409	1466
9657-28	3.25	3.1	74	467	14900	23572	2932	318
9657-51	3.33	7.8	60	357	11743	24749	2788	210
9657-55	3.42	12.0	45	259	8117	54586	12329	1243
9657-59	3.50	9.0	34	156	5869	44729	9033	928
9657-41	3.58	13.1	14	63	4145	58960	12838	1421
9657-71	3.67	29.2	3	7	2783	89410	22128	2474
10049-11	3.84	19.7	0	10	2032	88609	19740	1966
10049-21	4.00	31.0	3	13	2114	135943	32998	3375
10049-31	4.17	32.0	1	4	1909	156967	39893	4942
10049-41	4.33	6.0	4	14	1884	77134	11715	1480
10049-51	4.50	13.2	5	13	1775	115605	22165	2861
10049-61	4.67	21.7	5	14	1887	162619	35804	4700
10376-21	5.25	6.3	17	38	2112	133248	17780	2115
10376-31	5.58	15.7	16	32	2762	242423	39960	3863
10739-02	6.09	6.8	36	55	3680	260720	32733	2628
11005-50	6.51	19.2	13	36	5805	342250	41686	1805
10739-38	6.64	11.5	27	47	7942	380148	52527	4174
10733-N0	6.77	30.6	21	46	9013	468377	82410	7952
10733-N1	6.77	31.3	21	48	9081	470163	82462	7967
10733-N3	6.78	1.0	23	50	8311	350676	36324	1396
10733-N4	6.81	13.0	22	48	8903	406370	57171	4374

Figure 7: Table 1. from ACS ISR 2007-01. This Table shows the ACS low sensitivity populations for the positive and negative percentage bins with respect to the year and time after anneal (Time) for the F435W filter.

Comparing results in the F438W filter for both WFC3 and ACS, the latter has 3x as many low-sensitivity pixels, post-cooldown, in the < 1% bin than WFC3 (127,309 vs 402,997). The ACS WFC data was obtained over a longer time frame while the data quoted in this report is over an approximate 6 month

period. As Gilliland et al. observed, we also conclude that low-sensitivity pixels recover their losses within a few anneals, some as quickly as one anneal. The similarities between the ACS WFC and WFC3 UVIS detectors in relation to the low-sensitivity pixel populations might hint that these pixels are the result of radiation damage to the CCDs. ACS is 7 years older than WFC3 (installed March 2002 vs WFC3 in May 2009); if the low-sensitivity population is due to unavoidable radiation damage, this could explain why ACS exhibits a larger population than WFC3.

9 Discussion

The WFC3 UVIS detector has a population of low-sensitivity pixels that develop between anneals. The population that develops is different each month, i.e., the same pixels are not flipping between normal and low sensitivity. Like the hot pixel population, the pixels with low-sensitivity are largely reset with the anneal process; however, some recover spontaneously without an anneal. We see strong evidence for wavelength dependence in the population with the bluer filters exhibiting more low sensitivity pixels at the –2% level than the redder filters. Low-sensitivity pixels at the shorter wavelengths also typically require more anneals to recover normal sensitivity than low-sensitivity pixels at longer wavelengths. Preliminary analysis of low sensitivity pixels in the UV (filters F336W, F225W) suggests that the population is clumpy, i.e. pixels with low-sensitivity are not isolated events as they are at longer wavelengths. Further analysis is underway to better understand the behavior at UV wavelengths.

The presence of the low-sensitivity pixels across all wavelengths utilized by the UVIS detector should be a strong motivator for users to dither data. Dithering will help mitigate the effects from the lost charge in these pixel populations. Even though our UV analysis is preliminary and ongoing, our analysis strongly suggests that users observing extended sources, especially in the UV, should dither. Given the transient nature of the pixel population, without enough long-term data to confirm long-term repeat offending pixels we cannot flag these pixels as bad in the DQ array. Dithering is currently the best mitigation option available to observers.

10 Summary

- Transient pixels with low sensitivity have been identified and tracked within WFC3/UVIS internal flat field observations in the F814W, F438W, F336W, and F225W filters.
- The low sensitivity pixels are single, isolated pixels at long wavelengths, but sometimes form small clumps (2-4 pixels in size) at short wavelengths.
- The sensitivity loss (of order 1-2%) is greater at shorter wavelengths than at longer wavelengths.
- More low sensitivity pixels are detected at blue wavelengths than at red wavelengths but the total percentage of the UVIS detector affected by low sensitivity pixels is low. Pixels deviating by more than 2-3% range from 0.1% in F814W and F438W and from $\sim$ 3% up to 10% of the detector in F225W, depending on the time since the anneal procedure.
- The phenomenon is a multiplicative (i.e., not additive) effect, similar to what has been seen with the ACS/WFC detector.

- The low sensitivity population is a predominantly different set of pixels during each period between anneals, i.e., there is no 'flickering'.
- Most of the low-sensitivity pixels are reset by the monthly annealing process at all wavelengths. The efficacy of the reset does depend on the wavelength or the population bin. Some low-sensitivity pixels, especially at bluer wavelengths, require more than one anneal to reset completely. And while some pixels are technically considered to be reset, i.e., they recover to within 1% of their former value, many never recover completely to their former value.
- Currently, the best mitigation option is to dither, particularly for programs observing extended sources in the UV, where the low sensitivity pixels appear to be clumped.

Acknowledgments

The authors would like to thank Cheryl Pavlovsky, the initial investigator of this pixel population in the UVIS detector, and Jay Anderson, for his thorough review and helpful suggestions for this ISR.

Errata

This ISR was amended on 09/9/2014 to update Figures 10-13. The authors would like to thank Dr. Peter McCullough for pointing out an error in the figures. The corrected error does not affect the analysis or conclusions presented in this ISR.

References

M. Bourque & S. Baggett, 2013, WFC3 ISR 2013-09, "WFC3/UVIS Bowtie Monitor"

T. Brown, G. Hartig, S. Baggett, 2008, WFC3 ISR 2008-10, "WFC3 TV3 Testing: UVIS Window Contamination"

Gilliland R. L., Bohlin R., 2007, ACS ISR 2007-01, "Pixel-to-pixel Flate Field Changes on the WFC"

E. Sabbi, 2008, WFC3 ISR 2008-17, "UVIS Calsystem Photometric Filter Flat Field Atlas"

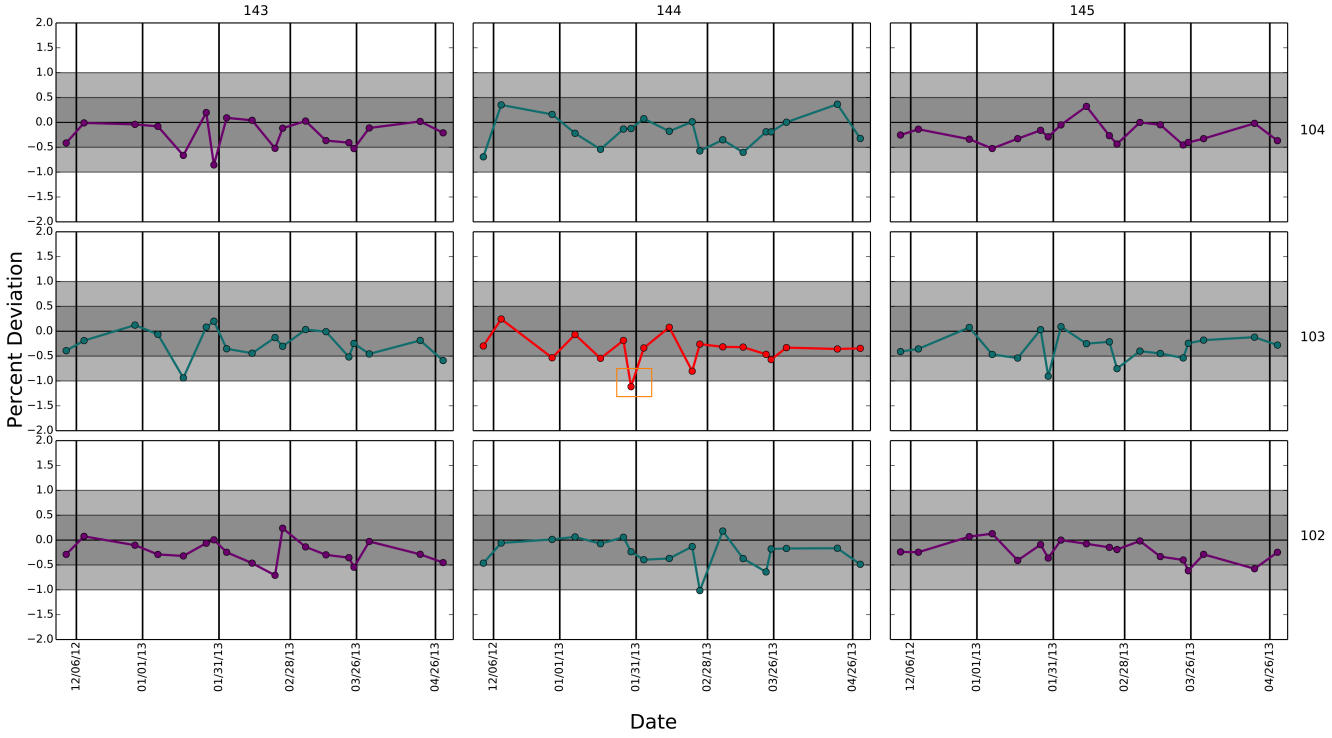

Figure 8: Pixel 144,103 (x,y) on chip 1 was identified as having low sensitivity < -1% in F814W.

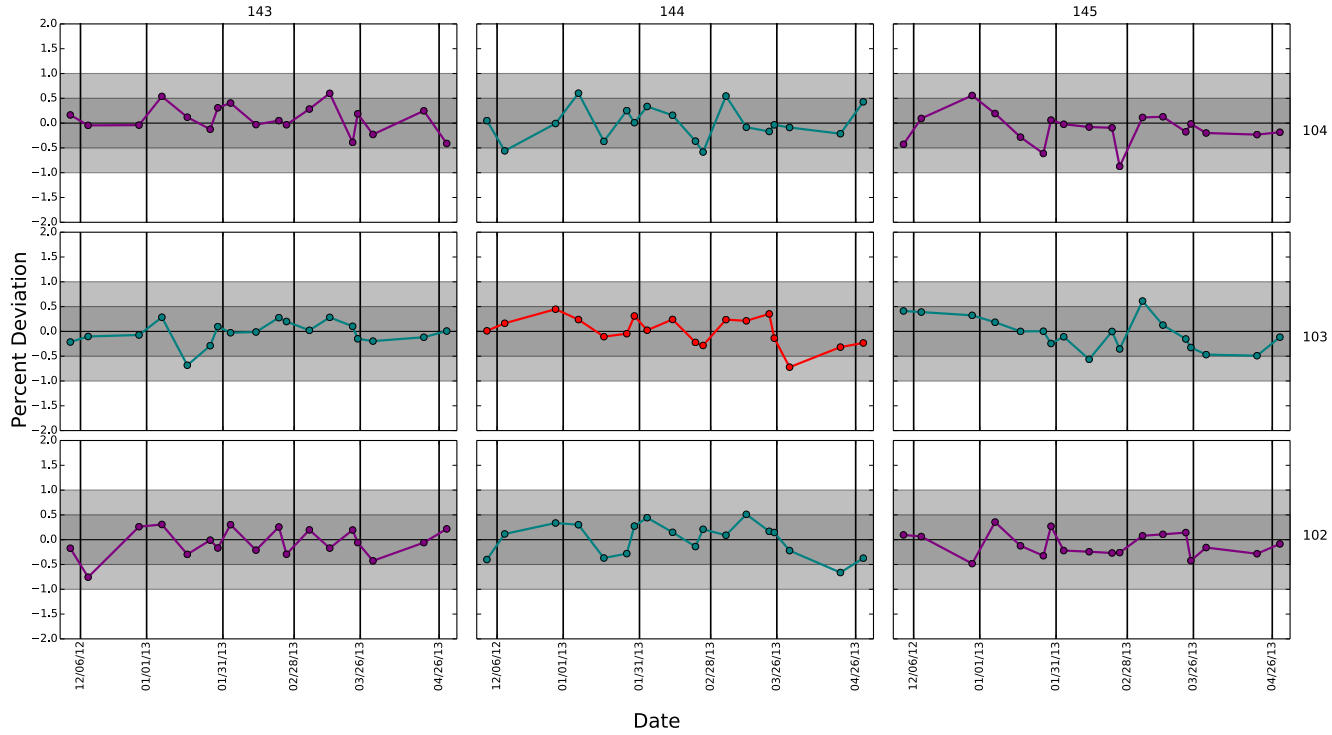

Figure 9: Pixel 144,103 (x,y) on chip 1 in F438W

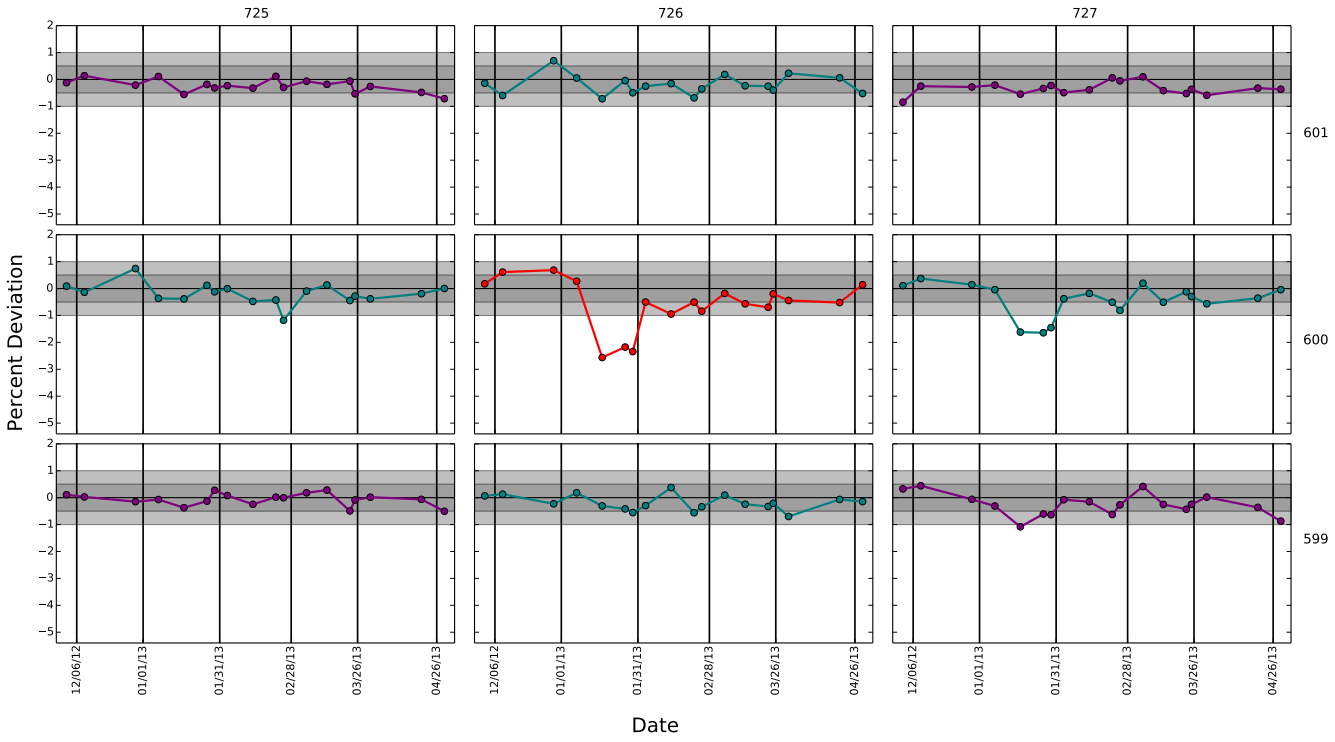

Figure 10: Pixel 726,600 (x,y) on chip 1 was identified as having low sensitivity < -2% in F814W.

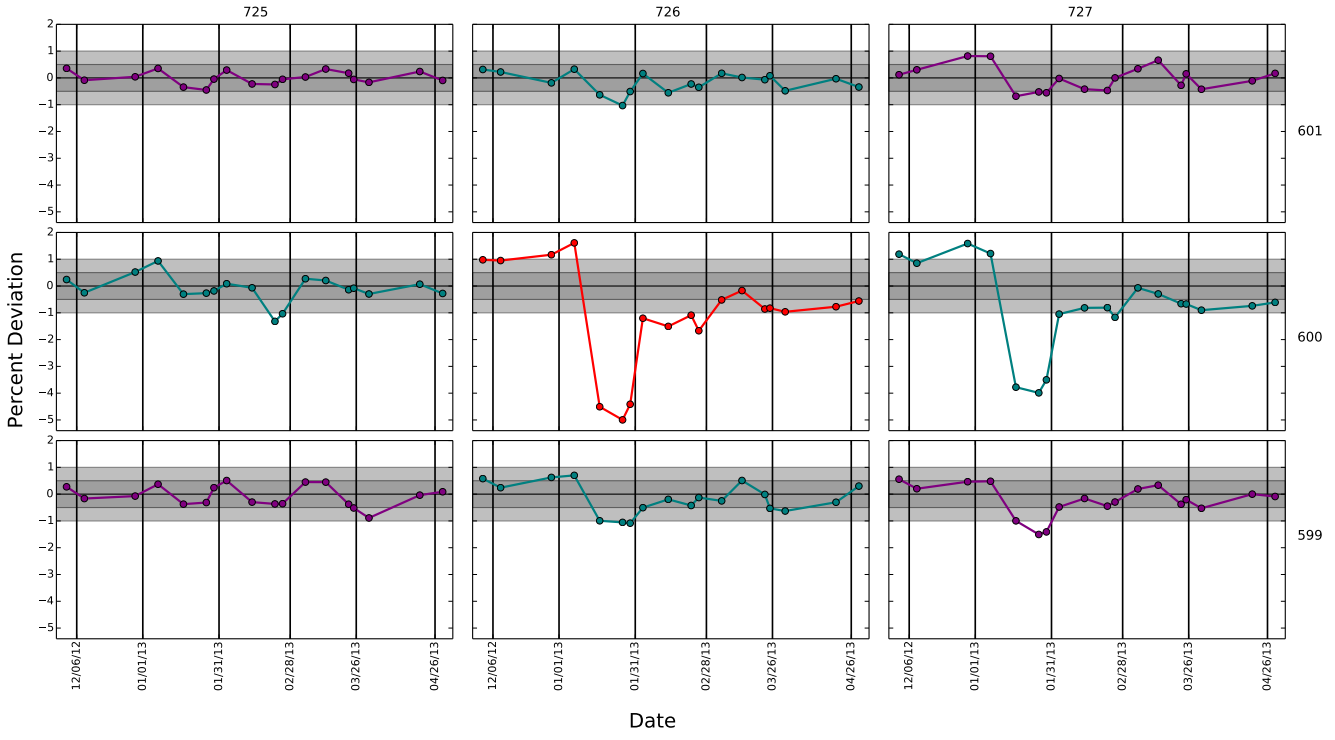

Figure 11: Pixel 726,600 (x,y) on chip 1 in F438W

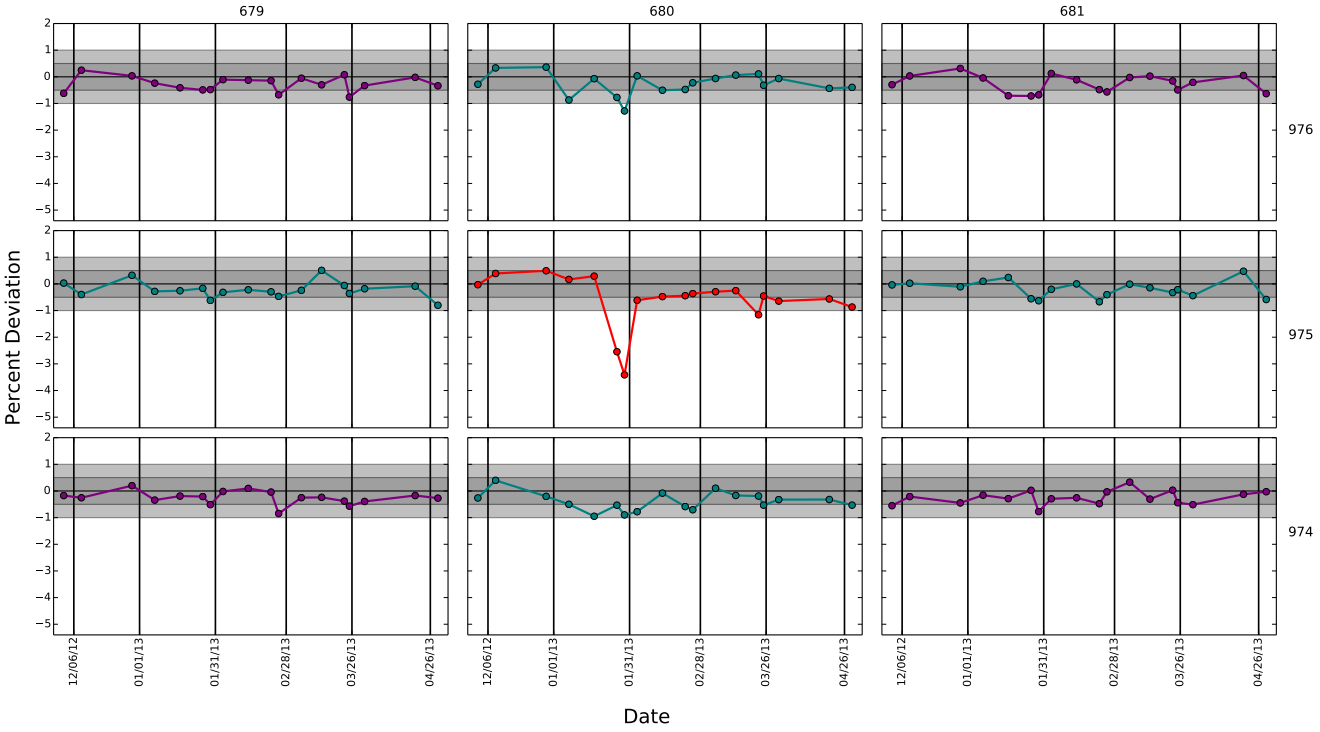

Figure 12: Pixel 680,975 (x,y) on chip 1 was identified as having low sensitivity < -4% in F814W.

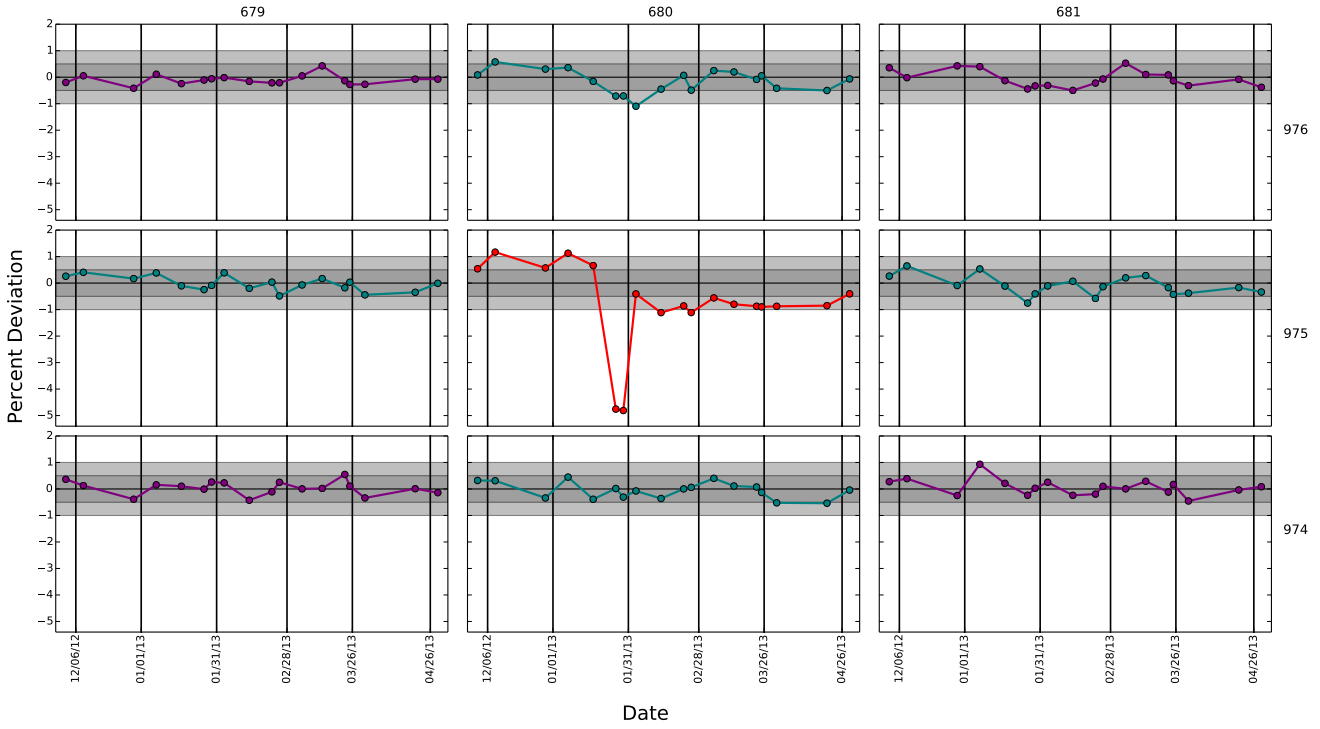

Figure 13: Pixel 680,975 (x,y) on chip 1 in F438W

Table A

Obs Date	Visit	Dataset	Exptime	Aperture	Filter
12/2/12	Visit 02	IC5Y02AYQ	18	UVIS	F225W
		IC5Y02AZQ	18	UVIS	F225W
		IC5Y02B1Q	18	UVIS	F225W
		IC5Y02B2Q	18	UVIS	F225W
		IC5Y02B4Q	58	UVIS	F336W
		IC5Y02B5Q	58	UVIS	F336W
		IC5Y02B7Q	58	UVIS	F336W
12/2/12	Visit 01	IC5Y01ZWQ	60	UVIS1-M512-SUB	F645N
		IC5Y01ZXQ	2	UVIS	F814W
		IC5Y01ZYQ	360	UVIS	F438W
		IC5Y01A1Q	360	UVIS	F438W
		IC5Y01A3Q	360	UVIS	F438W
		IC5Y01A5Q	360	UVIS	F438W
		IC5Y01A7Q	2	UVIS	F814W
		IC5Y01A9Q	2	UVIS	F814W
		IC5Y01AAQ	2	UVIS	F814W
12/9/12	Visit 04	IC5Y04IKQ	18	UVIS	F225W
		IC5Y04ILQ	18	UVIS	F225W
		IC5Y04INQ	18	UVIS	F225W
		IC5Y04IOQ	18	UVIS	F225W
		IC5Y04IQQ	58	UVIS	F336W
		IC5Y04IRQ	58	UVIS	F336W
		IC5Y04ITQ	58	UVIS	F336W
12/9/12	Visit 03	IC5Y03JWQ	60	UVIS1-M512-SUB	F645N
		IC5Y03JXQ	2	UVIS	F814W
		IC5Y03JYQ	360	UVIS	F438W
		IC5Y03K0Q	360	UVIS	F438W
		IC5Y03K2Q	360	UVIS	F438W
		IC5Y03K4Q	360	UVIS	F438W
		IC5Y03K6Q	2	UVIS	F814W
		IC5Y03K8Q	2	UVIS	F814W
		IC5Y03K9Q	2	UVIS	F814W

Obs Date	Visit	Dataset	Exptime	Aperture	Filter
12/29/12	Visit 06	IC5Y06EIQ	18	UVIS	F225W
		IC5Y06EJQ	18	UVIS	F225W
		IC5Y06ELQ	18	UVIS	F225W
		IC5Y06EMQ	18	UVIS	F225W
		IC5Y06EOQ	58	UVIS	F336W
		IC5Y06EPQ	58	UVIS	F336W
		IC5Y06ERQ	58	UVIS	F336W
12/29/12	Visit 05	IC5Y05E1Q	60	UVIS1-M512-SUB	F645N
		IC5Y05E2Q	2	UVIS	F814W
		IC5Y05E3Q	360	UVIS	F438W
		IC5Y05E5Q	360	UVIS	F438W
		IC5Y05E7Q	360	UVIS	F438W
		IC5Y05E9Q	360	UVIS	F438W
		IC5Y05EBQ	2	UVIS	F814W
		IC5Y05EDQ	2	UVIS	F814W
		IC5Y05EEQ	2	UVIS	F814W
1/7/13	Visit 07	IC5Y07F5Q	60	UVIS1-M512-SUB	F645N
		IC5Y07F6Q	2	UVIS	F814W
		IC5Y07F7Q	360	UVIS	F438W
		IC5Y07F9Q	360	UVIS	F438W
		IC5Y07FBQ	360	UVIS	F438W
		IC5Y07FDQ	360	UVIS	F438W
		IC5Y07FFQ	2	UVIS	F814W
		IC5Y07FHQ	2	UVIS	F814W
		IC5Y07FIQ	2	UVIS	F814W
1/17/13	Visit 08	IC5Y08ZWQ	60	UVIS1-M512-SUB	F645N
		IC5Y08ZXQ	2	UVIS	F814W
		IC5Y08ZYQ	360	UVIS	F438W
		IC5Y08A1Q	360	UVIS	F438W
		IC5Y08A3Q	360	UVIS	F438W
		IC5Y08A5Q	360	UVIS	F438W
		IC5Y08A7Q	2	UVIS	F814W
		IC5Y08A9Q	2	UVIS	F814W
		IC5Y08AAQ	2	UVIS	F814W
1/25/13	Visit 10	IC5Y10DKQ	60	UVIS1-M512-SUB	F645N
		IC5Y10DLQ	2	UVIS	F814W
		IC5Y10DMQ	360	UVIS	F438W
		IC5Y10DOQ	360	UVIS	F438W
		IC5Y10DQQ	360	UVIS	F438W
		IC5Y10DSQ	360	UVIS	F438W
		IC5Y10DUQ	2	UVIS	F814W
		IC5Y10DWQ	2	UVIS	F814W
		IC5Y10DXQ	2	UVIS	F814W

Obs Date	Visit	Dataset	Exptime	Aperture	Filter
1/26/13	Visit 09	IC5Y09JOQ	60	UVIS1-M512-SUB	F645N
		IC5Y09JPQ	2	UVIS	F814W
		IC5Y09JQQ	360	UVIS	F438W
		IC5Y09JSQ	360	UVIS	F438W
		IC5Y09JUQ	360	UVIS	F438W
		IC5Y09JWQ	360	UVIS	F438W
		IC5Y09JYQ	2	UVIS	F814W
		IC5Y09K0Q	2	UVIS	F814W
		IC5Y09K1Q	2	UVIS	F814W
2/3/13	Visit 11	IC5Y11MIQ	60	UVIS1-M512-SUB	F645N
		IC5Y11MJQ	2	UVIS	F814W
		IC5Y11MKQ	360	UVIS	F438W
		IC5Y11MMQ	360	UVIS	F438W
		IC5Y11MOQ	360	UVIS	F438W
		IC5Y11MQQ	360	UVIS	F438W
		IC5Y11MSQ	2	UVIS	F814W
		IC5Y11MUQ	2	UVIS	F814W
		IC5Y11MVQ	2	UVIS	F814W
2/13/13	Visit 12	IC5Y12OVQ	60	UVIS1-M512-SUB	F645N
		IC5Y12OWQ	2	UVIS	F814W
		IC5Y12OXQ	360	UVIS	F438W
		IC5Y12OZQ	360	UVIS	F438W
		IC5Y12P1Q	360	UVIS	F438W
		IC5Y12P3Q	360	UVIS	F438W
		IC5Y12P5Q	2	UVIS	F814W
		IC5Y12P7Q	2	UVIS	F814W
		IC5Y12P8Q	2	UVIS	F814W
2/22/13	Visit 14	IC5Y14PLQ	60	UVIS1-M512-SUB	F645N
		IC5Y14PMQ	2	UVIS	F814W
		IC5Y14PNQ	360	UVIS	F438W
		IC5Y14PPQ	360	UVIS	F438W
		IC5Y14PRQ	360	UVIS	F438W
		IC5Y14PTQ	360	UVIS	F438W
		IC5Y14PVQ	2	UVIS	F814W
		IC5Y14PXQ	2	UVIS	F814W
		IC5Y14PYQ	2	UVIS	F814W
2/25/13	Visit 13	IC5Y13FXQ	60	UVIS1-M512-SUB	F645N
		IC5Y13FYQ	2	UVIS	F814W
		IC5Y13FZQ	360	UVIS	F438W
		IC5Y13G1Q	360	UVIS	F438W
		IC5Y13G3Q	360	UVIS	F438W
		IC5Y13G5Q	360	UVIS	F438W
		IC5Y13G7Q	2	UVIS	F814W
		IC5Y13G9Q	2	UVIS	F814W
		IC5Y13GAQ	2	UVIS	F814W

Obs Date	Visit	Dataset	Exptime	Aperture	Filter
3/6/13	Visit 15	IC5Y15CLQ	60	UVIS1-M512-SUB	F645N
		IC5Y15CMQ	2	UVIS	F814W
		IC5Y15CNQ	360	UVIS	F438W
		IC5Y15CPQ	360	UVIS	F438W
		IC5Y15CRQ	360	UVIS	F438W
		IC5Y15CTQ	360	UVIS	F438W
		IC5Y15CVQ	2	UVIS	F814W
		IC5Y15CXQ	2	UVIS	F814W
		IC5Y15CYQ	2	UVIS	F814W
3/14/13	Visit 16	IC5Y16Y9Q	60	UVIS1-M512-SUB	F645N
		IC5Y16YAQ	2	UVIS	F814W
		IC5Y16YBQ	360	UVIS	F438W
		IC5Y16YDQ	360	UVIS	F438W
		IC5Y16YFQ	360	UVIS	F438W
		IC5Y16YHQ	360	UVIS	F438W
		IC5Y16YJQ	2	UVIS	F814W
		IC5Y16YLQ	2	UVIS	F814W
		IC5Y16YMQ	2	UVIS	F814W
3/23/13	Visit 18	IC5Y18EMQ	60	UVIS1-M512-SUB	F645N
		IC5Y18ENQ	2	UVIS	F814W
		IC5Y18EOQ	360	UVIS	F438W
		IC5Y18EQQ	360	UVIS	F438W
		IC5Y18ESQ	360	UVIS	F438W
		IC5Y18EUQ	360	UVIS	F438W
		IC5Y18EWQ	2	UVIS	F814W
		IC5Y18EYQ	2	UVIS	F814W
		IC5Y18EZQ	2	UVIS	F814W
3/25/13	Visit 17	IC5Y17F6Q	60	UVIS1-M512-SUB	F645N
		IC5Y17F7Q	2	UVIS	F814W
		IC5Y17F8Q	360	UVIS	F438W
		IC5Y17FAQ	360	UVIS	F438W
		IC5Y17FCQ	360	UVIS	F438W
		IC5Y17FEQ	360	UVIS	F438W
		IC5Y17FGQ	2	UVIS	F814W
		IC5Y17FIQ	2	UVIS	F814W
		IC5Y17FJQ	2	UVIS	F814W
3/31/13	Visit 20	IC5Y20GFQ	18	UVIS	F225W
		IC5Y20GGQ	18	UVIS	F225W
		IC5Y20GIQ	18	UVIS	F225W
		IC5Y20GJQ	18	UVIS	F225W
		IC5Y20GLQ	58	UVIS	F336W
		IC5Y20GMQ	58	UVIS	F336W
		IC5Y20GOQ	58	UVIS	F336W

Obs Date	Visit	Dataset	Exptime	Aperture	Filter
3/31/13	Visit 19	IC5Y19FLQ	60	UVIS1-M512-SUB	F645N
		IC5Y19FMQ	2	UVIS	F814W
		IC5Y19FNQ	360	UVIS	F438W
		IC5Y19FPQ	360	UVIS	F438W
		IC5Y19FRQ	360	UVIS	F438W
		IC5Y19FTQ	360	UVIS	F438W
		IC5Y19FVQ	2	UVIS	F814W
		IC5Y19FXQ	2	UVIS	F814W
		IC5Y19FYQ	2	UVIS	F814W
4/20/13	Visit 22	IC5Y22AAQ	18	UVIS	F225W
		IC5Y22ABQ	18	UVIS	F225W
		IC5Y22ADQ	18	UVIS	F225W
		IC5Y22AEQ	18	UVIS	F225W
		IC5Y22AGQ	58	UVIS	F336W
		IC5Y22AHQ	58	UVIS	F336W
		IC5Y22AJQ	58	UVIS	F336W
4/20/13	Visit 21	IC5Y21ZQQ	60	UVIS1-M512-SUB	F645N
		IC5Y21ZRQ	2	UVIS	F814W
		IC5Y21ZSQ	360	UVIS	F438W
		IC5Y21ZUQ	360	UVIS	F438W
		IC5Y21ZWQ	360	UVIS	F438W
		IC5Y21ZYQ	360	UVIS	F438W
		IC5Y21A1Q	2	UVIS	F814W
		IC5Y21A3Q	2	UVIS	F814W
		IC5Y21A4Q	2	UVIS	F814W
4/20/13	Visit 22	IC5Y22AAQ	18	UVIS	F225W
		IC5Y22ABQ	18	UVIS	F225W
		IC5Y22ADQ	18	UVIS	F225W
		IC5Y22AEQ	18	UVIS	F225W
		IC5Y22AGQ	58	UVIS	F336W
		IC5Y22AHQ	58	UVIS	F336W
		IC5Y22AJQ	58	UVIS	F336W
4/20/13	Visit 21	IC5Y21ZQQ	60	UVIS1-M512-SUB	F645N
		IC5Y21ZRQ	2	UVIS	F814W
		IC5Y21ZSQ	360	UVIS	F438W
		IC5Y21ZUQ	360	UVIS	F438W
		IC5Y21ZWQ	360	UVIS	F438W
		IC5Y21ZYQ	360	UVIS	F438W
		IC5Y21A1Q	2	UVIS	F814W
		IC5Y21A3Q	2	UVIS	F814W
		IC5Y21A4Q	2	UVIS	F814W

Obs Date	Visit	Dataset	Exptime	Aperture	Filter
4/29/13	Visit 24	IC5Y24E8Q	18	UVIS	F225W
		IC5Y24E9Q	18	UVIS	F225W
		IC5Y24EBQ	18	UVIS	F225W
		IC5Y24ECQ	18	UVIS	F225W
		IC5Y24EEQ	58	UVIS	F336W
		IC5Y24EFQ	58	UVIS	F336W
		IC5Y24EHQ	58	UVIS	F336W
4/29/13	Visit 23	IC5Y23DJQ	60	UVIS1-M512-SUB	F645N
		IC5Y23DKQ	2	UVIS	F814W
		IC5Y23DLQ	360	UVIS	F438W
		IC5Y23DNQ	360	UVIS	F438W
		IC5Y23DPQ	360	UVIS	F438W
		IC5Y23DRQ	360	UVIS	F438W
		IC5Y23DTQ	2	UVIS	F814W
		IC5Y23DVQ	2	UVIS	F814W
		IC5Y23DWQ	2	UVIS	F814W

Table A: All data for cycle 20 calibration program 13169.